Tuning the Optical and Photoelectrochemical Properties of Surface-Modified TiO_2

*Radim Beranek and Horst Kisch**

Institut für Anorganische Chemie der Universität Erlangen-Nürnberg, Egerlandstr.1, D-91058 Erlangen, Germany

Supplementary Information

1. X-Ray Diffractometry

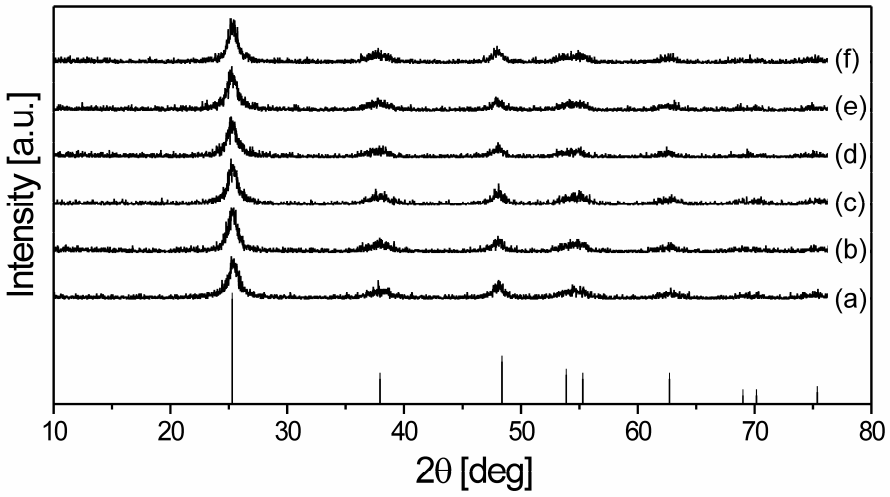

Figure S1. XRD spectra of unmodified TiO_2 (a) and TiO_2-N modified at 300 °C (b), 350 °C (c), 400 °C (d), 450 °C (e), and 500 °C (f). Spectra are off-set for clarity. Vertical lines show a literature pattern of anatase (ASTM file card No. 01-0562)

2. Infrared Spectroscopy

FT-IR transmission spectra (Fig. S2) were obtained using a Perkin-Elmer PE-16PC FT-IR spectrometer against an air background. The samples were pressed pellets of a mixture of the powder with KBr.

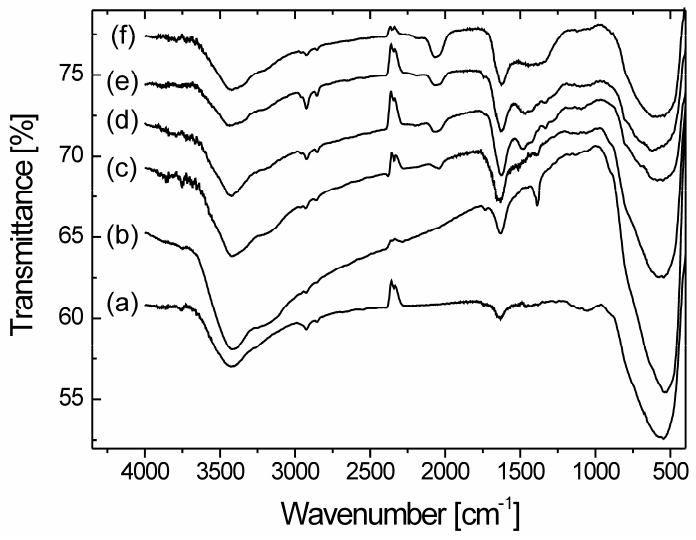

Figure S2. FT-IR spectra of unmodified TiO_2 (a) and TiO_2-N modified at 300 °C (b), 350 °C (c), 400 °C (d), 450 °C (e), and 500 °C (f). Spectra are off-set for clarity.

Several peaks related to TiO_2 are observed in all samples. The broad band centered at 500-600 cm^{-1} is likely due to the vibration of the Ti–O bonds in the TiO_2 lattice.[S1] The peaks at 1620-1630 cm^{-1} and the broad peaks appearing at 3100–3600 cm^{-1} are assigned to vibrations of hydroxyl groups.[S1-3] In modified samples these peaks overlap with broad bands of the stretching and deformation modes of NH_x groups.[S2,4] The multiple bands at 1200-1550 cm^{-1} and the peaks at ~2060 cm^{-1} are assumed to be due to the species containing CN bonds, such as cyanamide, carbodiimide, cyanuric acid, and related compounds coming from the decomposition products of urea.[S5-7] Alternatively, the bands at 1200-1550 cm^{-1} could be also ascribed to nitrogen oxide species.[S8]

3. Thermogravimetric analysis (TGA)

Thermal analysis of TiO_2-N modified at 400 °C was performed using a Universal V2.6D TA Instrument in a nitrogen atmosphere in the temperature range of 24–1000 °C and a heating rate of 10 °C/min with a 60 min isothermal step at 200 °C. Enhanced weight loss above 450 °C indicates more intense desorption of surface species (Fig. S3).

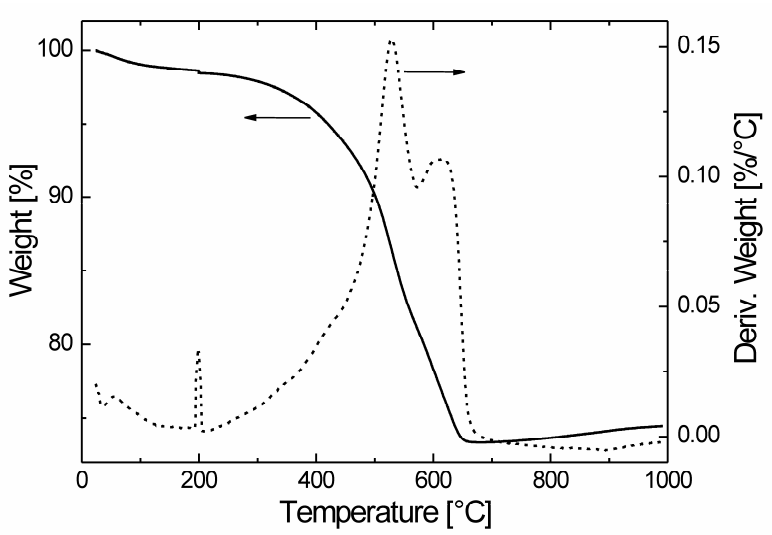

Figure S3. TGA thermogram of TiO_2-N modified at 400 °C. Enhanced weight loss above 450 °C indicates more intense desorption of surface species.

4. Removal of surface modification through treatment in boiling NaOH (5 M)

300 mg of TiO_2-N modified at 400 °C (yellow powder; bandgap = 2.29 eV) was treated in boiling NaOH (5 M) for 1 hour and subsequently washed twice with water and dried at 100 °C. The resulting powder (0.1 wt % N; 0.6 wt % C) was white and exhibited bandgap of 3.18 eV (Fig. S4) – a typical bandgap of unmodified titania, and induced negligible photocurrents in the visible when deposited on ITO-glass.

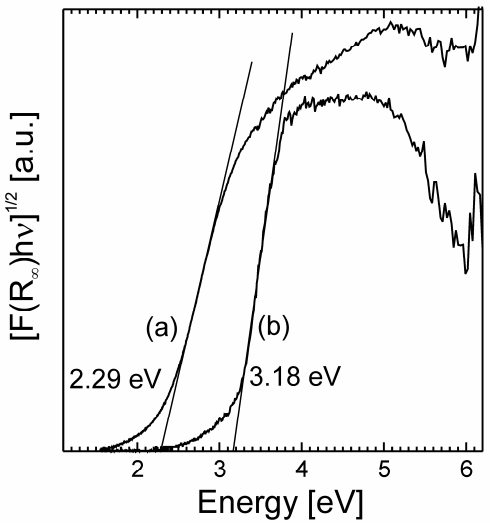

Figure S4. Bandgap determination using $[F(R_\infty)h\nu]^{1/2}$ vs. $h\nu$ plots (assuming an indirect optical transition) for TiO_2-N modified at 400 °C before (a), and after treatment in boiling NaOH (5 M) for 1 hour.

5. Ti2p XPS spectra upon sputtering with Ar^+ ions

Figure S5 shows the influence of the Ar^+ ion sputtering on the Ti2p XPS spectra. The apparent broadening of the $Ti2p_{3/2}$ peak is due to the partial reduction of surface Ti^{4+} species to intermediate oxidation states. The broadening clearly increases with increasing sputtering time (Fig. S5A). After 10 nm thick layer was sputtered off the lower binding energy $Ti2p_{3/2}$ subpeak obtained by deconvolution exhibits the value of 455.5 eV – a typical value for Ti^{3+} species in titanium nitride.[S9] Reduction of surface Ti^{4+} species upon sputtering was observed also for unmodified TiO_2 (Fig. S5B). This behavior is in the literature reported to be caused by preferential sputtering of oxygen leading to generation of defects (oxygen vacancies).[S10-13]

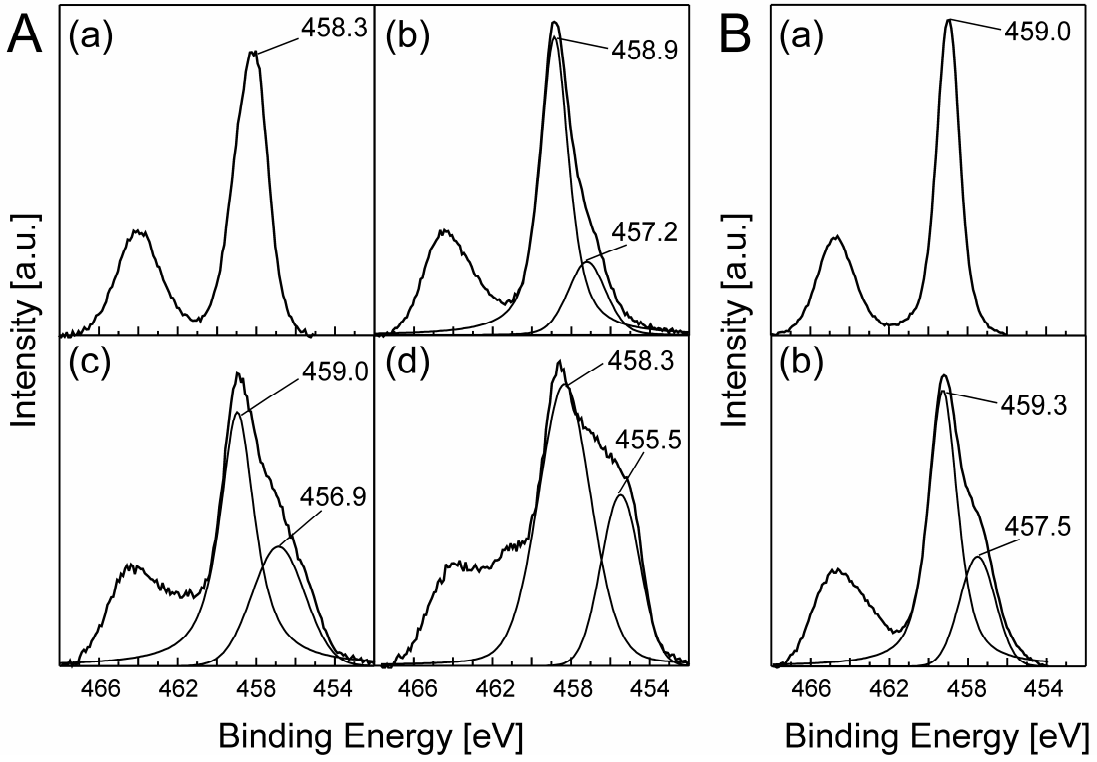

Figure S5. (A) High-resolution Ti2p XPS spectra of TiO_2-N modified at 400 °C recorded before (a) and after sputtering with Ar^+ ions to remove the top layer with a thickness of about 1 nm (b), 5 nm (c), and 10 nm (d). (B) Ti2p XPS spectra of unmodified TiO_2 before (a) and after (b) sputtering (5 nm).

6. Influence of the starting material properties on the modification

In order to investigate the influence of the starting material properties on the modification, the starting material (Hombikat UV 100, Sachtleben, Germany) was first heat pretreated at 800 °C in air for 3 hours and then modified by the standard procedure at 400 °C. Table S1 summarizes the properties of untreated and heat-pretreated TiO_2 before and after modification.

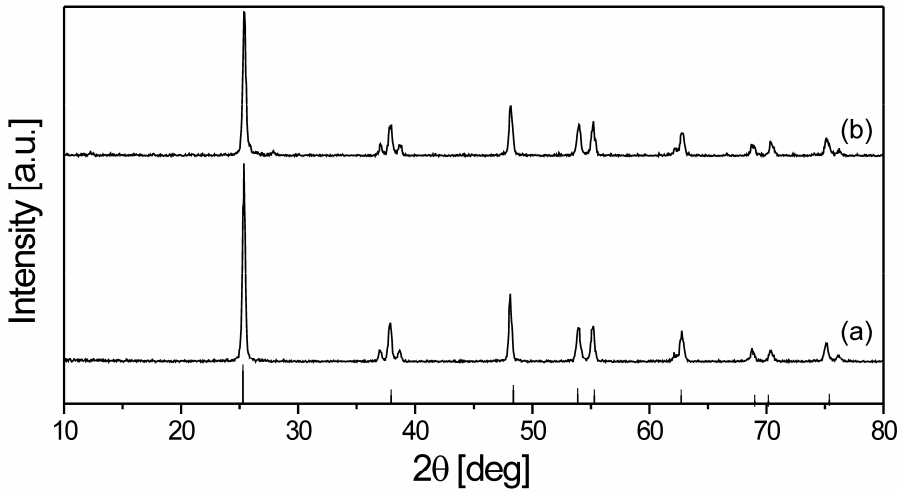

Figure S6. XRD spectra of TiO_2 preheated at 800 °C in air for 3 hours before (a) and after modification. Spectra are off-set for clarity. Vertical lines show a literature pattern of anatase (ASTM file card No. 01-0562).

Table S1. Influence of Various Parameters on Modification: Crystallite Size (before/after modification);[a] Surface Area (before/after modification);[b] Surface OH-groups;[c] Nitrogen and Carbon Content[d] (after modification)

Starting Material Pretreatment	Crystallite Size [nm]	Surface Area [m^2/g]	Surface OH-groups [10^{-4} mol/g]	N [wt %]	C [wt %]
–	8 / 8	282 / 53	17.6	15.5	7.9
800 °C in air (3hours)	32 / 31	14 / 12	3.2	5.6	2.9

[a] calculated from Scherrer formula; [b] BET method; [c] from TGA analysis; [d] Elemental analysis

The pretreated material retained the anatase structure and exhibited ~ 4 times larger crystallite size, ~ 20 times lower surface area and ~ 5.5 times lower concentration of surface OH-groups. Surface OH-groups were determined by TGA analysis (Universal V2.6D TA Instrument; nitrogen atmosphere; temperature range: 24–1000 °C ; heating rate = 10 °C/min with a 60 min isothermal step at 200 °C) assuming that the weight loss between 200 °C and 1000 °C is due to dehydroxylation of the surface. After modification, the pretreated material contained ~ 2.7 times lower amount of nitrogen and carbon and exhibited a larger bandgap of 2.77 eV in contrast to 2.29 eV of the material modified without a heat pretreatment (Fig. S7).

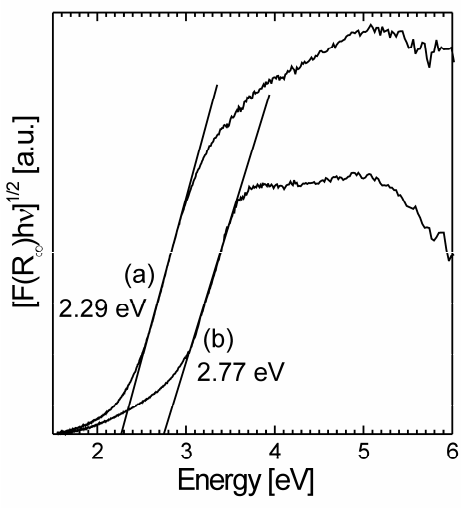

Figure S7. Bandgap determination using $[F(R_\infty)h\nu]^{1/2}$ vs. $h\nu$ plots (assuming an indirect optical transition) for TiO_2-N modified at 400 °C without (a), and with calcination pretreatment in air at 800 °C for 3 hours (b).

7. Determination of band edges – quasi-Fermi level measurements

For heavily doped n-type metal oxides like TiO_2, the lower conduction band edge, E_c, practically merges with the quasi-Fermi level for electrons, ${}_nE_F^*$, ($|E_c - {}_nE_F^*| < 0.1$ V).[S14-16] The values of ${}_nE_F^*$ were determined by the method of Roy.[S17,18] In short, we recorded the pH dependence of the potential of a Pt electrode immersed in an irradiated (Osram XBO 150 W xenon arc lamp) suspension of a semiconductor in the presence of an electron acceptor with pH-independent reduction potential. One of two different electron acceptors were used: MV^{2+} (methyl viologen; 1,1'-dimethyl-4,4'-bipyridinium dichloride; $E_{MV^{2+/+\bullet}} = -0.45$ V vs. NHE)[S19] and DP^{2+} (4,5-dihydro-3a,5a-diaza-pyrene dibromide; $E_{DP^{2+/+\bullet}} = -0.27$ V vs. NHE).[S20-23] The inflection point (pH_0) of the potential-pH curve (Fig. S8) determines the pH value at which ${}_nE_F^*$ coincides with $E_{MV^{2+/+\bullet}}$ or $E_{DP^{2+/+\bullet}}$. Assuming Nernstian shift of band edges[S16,24] the values of ${}_nE_F^*$ at pH = 7 can be then obtained from equations ${}_nE_F^* = E_{MV^{2+/+\bullet}} + 0.059\ (pH_0 - 7)$ or ${}_nE_F^* = E_{DP^{2+/+\bullet}} + 0.059\ (pH_0 - 7)$, respectively.

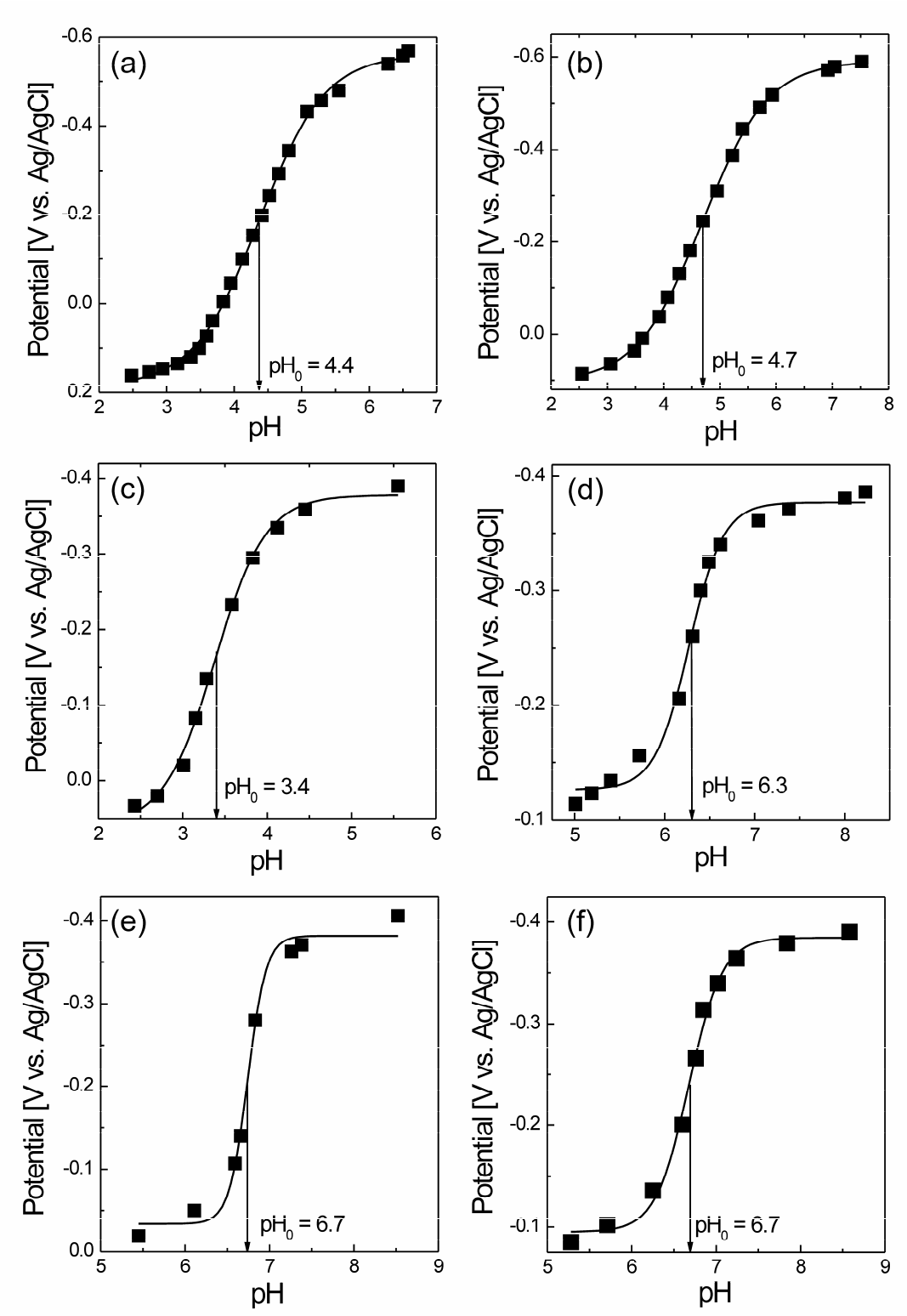

Figure S8. pH dependence of the potential of a Pt electrode immersed in an irradiated suspension of unmodified TiO_2 (a) and TiO_2-N modified at 300 °C (b), 350 °C (c), 400 °C (d), 450 °C (e), and 500 °C (f) in the presence of $(MV)Cl_2$ (a, b) or $(DP)Br_2$ (c-f).

8. Photocurrent transients

Figure S9 shows raw photocurrent spectra measured under intermittent irradiation as a function of irradiation wavelength (without correction for the change of light intensity) in $LiClO_4$ (0.1 M) without and with addition of KI (0.1 M). The insets show photocurrent transients at λ = 400 nm; the spike-like shape of the transient in absence of iodide is a typical fingerprint of surface recombination processes.[S24-29] Photogenerated holes are trapped too deep in the bandgap to induce efficient water oxidation (E ~ 2.0 V vs. NHE)[S19] and accumulate therefore at the surface. This increases the probability that they capture conduction band electrons, recombine and do not contribute to photocurrent. Accordingly, the recombination manifests itself by photocurrent decay after switching-on the light. The transients recorded in the presence of iodide indicate that more easily oxidizable iodide (E ~ 1.3 V vs. NHE)[S19] reacts more readily with surface-trapped holes. Thus the surface recombination is suppressed and the rapid photocurrent decay after switching-on the light is absent.

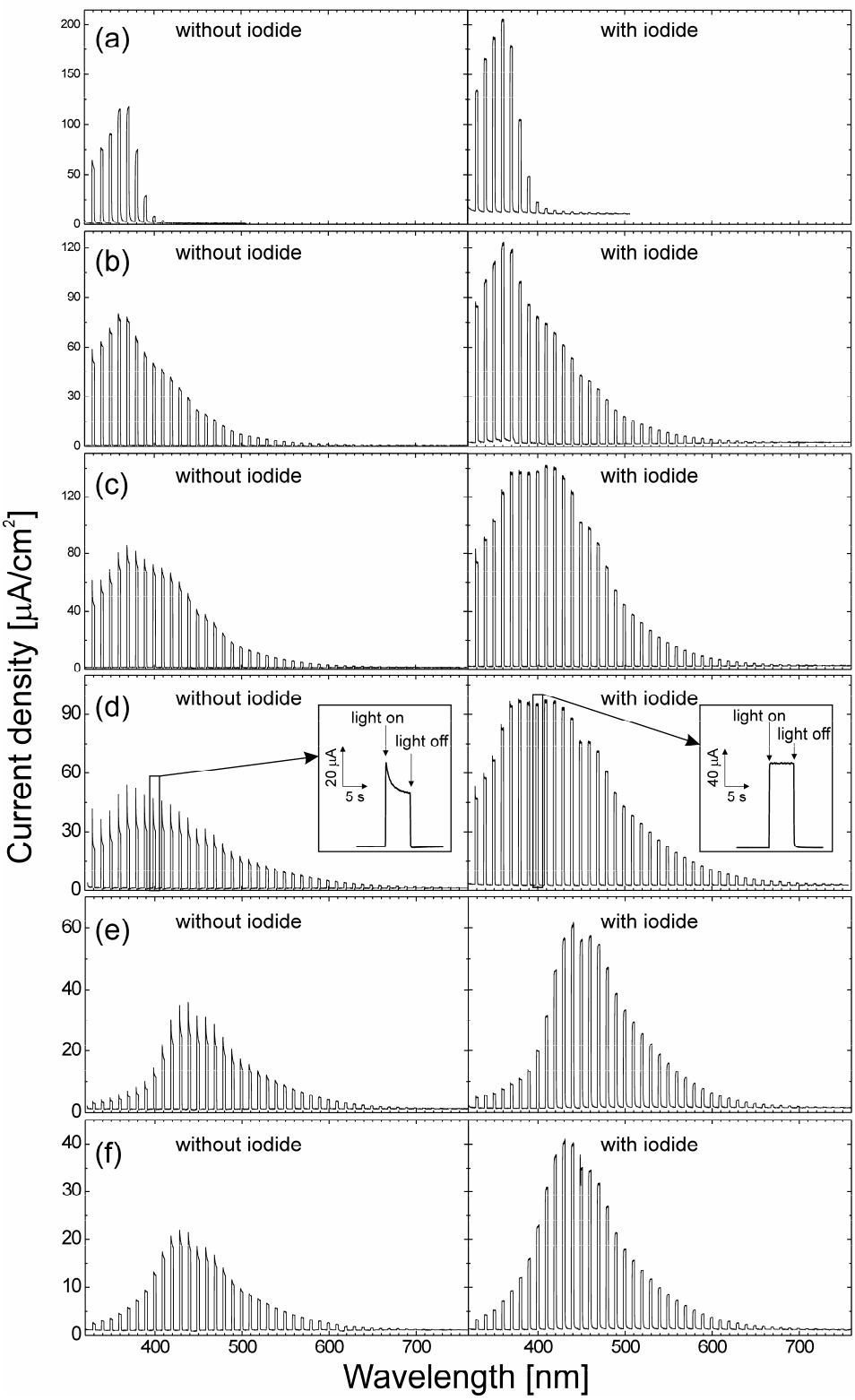

Figure S9. Photocurrent measured under intermittent irradiation as a function of irradiation wavelength (without correction for the change of light intensity) in $LiClO_4$ (0.1 M) without and with addition of KI (0.1 M): unmodified TiO_2 (a), TiO_2-N modified at 300 °C (b), 350 °C (c), 400 °C (d), 450 °C (e), and 500 °C (f). The insets show photocurrent transients at λ = 400 nm.

8. References

(S1) Gao, Y.; Masuda, Y.; Peng, Z.; Yonezawa, T.; Koumoto, K. *J. Mater. Chem.* **2003**, *13*, 608.

(S2) Nakamoto, K. *Infrared and Raman Spectra of Inorganic and Coordination Compounds*; John Wiley & Sons: New York, 1986.

(S3) Klingenberg, B.; Vannice, M. A. *Chem. Mater.* **1996**, *8*, 2755.

(S4) Khabashesku, V. N.; Zimmerman, J. L.; Margrave, J. L. *Chem. Mater.* **2000**, *12*, 3264.

(S5) Hauck, P.; Jentys, A.; Lercher, J. A. *Appl. Catal., B* **2007**, *70*, 91.

(S6) Guo, Q.; Xie, Y.; Wang, X.; Zhang, S.; Hou, T.; Lu, S. *Chem. Commun.* **2004**, 26.

(S7) Schaber, P. M.; Colson, J.; Higgins, S.; Thielen, D.; Anspach, B.; Brauer, J. *Thermochim. Acta* **2004**, *424*, 131.

(S8) Navio, J. A.; Cerrillos, C.; Real, C. *Surf. Interface Anal.* **1996**, *24*, 355.

(S9) Saha, N. C.; Tompkins, H. G. *J. Appl. Phys.* **1992**, *72*, 3072.

(S10) Göpel, W.; Anderson, J. A.; Frankel, D.; Jaehnig, M.; Phillips, K.; Schaefer, J. A.; Rocker, G. *Surf. Sci.* **1984**, *139*, 333.

(S11) Bardi, U.; Tamura, K.; Owari, M.; Nihei, Y. *Appl. Surf. Sci.* **1988**, *32*, 352.

(S12) Mayer, J. T.; Diebold, U.; Madey, T. E.; Garfunkel, E. *J. Electron Spectrosc. Relat. Phenom.* **1995**, *73*, 1.

(S13) Kunze, J.; Ghicov, A.; Hildebrand, H.; Macak, J. M.; Traveira, L.; Schmuki, P. *Z. Phys. Chem.* **2005**, *219*, 1561.

(S14) Butler, M. A.; Ginley, D. S. *Chem. Phys. Lett.* **1977**, *47*, 319.

(S15) Butler, M. A.; Ginley, D. S. *J. Electrochem. Soc.* **1978**, *125*, 228.

(S16) Morrison, S. R. *Electrochemistry at Semiconductor and Oxidized Metal Electrodes*; Plenum Press: New York, 1980.

(S17) Roy, A. M.; De, G. C.; Sasmal, N.; Bhattacharyya, S. S. *Int. J. Hydrogen Energy* **1995**, *20*, 627.

(S18) Kisch, H.; Burgeth, G.; Macyk, W. *Adv. Inorg. Chem.* **2004**, *56*, 241.

(S19) Wardman, P. *J. Phys. Chem. Ref. Data* **1989**, *18*, 1637.

(S20) Hünig, S.; Gross, J. *Tetrahedron Lett.* **1968**, *9*, 2599.

(S21) Hünig, S.; Gross, J.; Lier, E. F.; Quast, H. *Liebigs Ann. Chem.* **1973**, *1973*, 339.

(S22) Summers, L. A. *Tetrahedron* **1968**, *24*, 5433.

(S23) Gärtner, M. PhD thesis, Friedrich-Alexander-Universität Erlangen-Nürnberg, Erlangen, 2005.

(S24) Beranek, R.; Kisch, H. *Electrochem. Commun.* **2007**, *9*, 761.

(S25) Abrantes, L. M.; Peter, L. M. *J. Electroanal. Chem. Interf. Electrochem.* **1983**, *150*, 593.

(S26) Peter, L. M. *Chem. Rev.* **1990**, *90*, 753.

(S27) Tafalla, D.; Salvador, P.; Benito, R. M. *J. Electrochem. Soc.* **1990**, *137*, 1810.

(S28) Salvador, P.; Garcia Gonzalez, M. L.; Munoz, F. *J. Phys. Chem.* **1992**, *96*, 10349.

(S29) Hagfeldt, A.; Lindstroem, H.; Soedergren, S.; Lindquist, S.-E. *J. Electroanal. Chem.* **1995**, *381*, 39.